Supporting Information

Multifunctional Cobalt Metal Organic Framework luminescent probe for efficient sensing of $Cr_2O_7^{2-}$, MnO_4^- and Nucleobases

Ritu Ladhi [a], Deepika Rani, [a,b], Monika Singh[a]*

[a] Institute of Nano Science and Technology, Knowledge City, Sector-81, Mohali-140306, Punjab, INDIA

[b] Department of Chemistry, Panjab University, Chandigarh, INDIA

*Corresponding author: monika@inst.ac.in

Contents

Section S1: General information

Materials The reactants and solvents used in the procedure are obtained commercially from Sigma, CDH Fine chemicals and LobaChemei and used as purchased without any further purification

Physical Measurements FT-IR spectra were recorded on a PerkinElmer Spectrum I spectrometer with samples prepared as KBr pellets in the range of 4000-400 cm^{-1}. The solid state (DRS) and solution state UV-Vis spectra of compound and analyte were explored by UV/Vis spectrophotometer (Shimadzu UV-2600). The morphological studies were carried out by field emission scanning electron microscopy (FESEM) on a JEOL JSM-7600F system. TGA analysis was carried out using Perkin–Elmer Pyris 1 model on well ground samples in flowing nitrogen atmosphere at a heating rate of 10 °C/min. Emission spectra were recorded using an EDINBURGH instrument FS5 spectrophotometer. Time-resolved lifetime decay profiles were measured using photoluminescence Fluorolog 3-221 (Horiba Scientific) single photon counting controller. Powder X-ray diffraction analysis was carried out on a Bruker D8-Advance Eco Diffractometer using Ni-filtered Cu Kα radiation at room temperature. The data were collected over the range of $5° < 2\theta < 80°$ with a step size of 0.01°. The BET nitrogen isotherm analysis was carried out on Quantachrome ASiQwin at 300 K.

Single-Crystal X-ray Data Collection and Refinements The structural analysis was carried out by Single crystal XRD on a CMOS based Bruker D8 Venture PHOTON 100 diffractometer equipped with a INCOATEC micro-focus source with graphite monochromated Mo Kα radiation ($\lambda = 0.71073$ Å) operating at 50 kV and 30 mA. The crystal structures were solved by using SHELXS97 or SHELXT[1] and were refined using SHELXL97[2] through Olex2 suite.[3]All the hydrogen atoms were geometrically fixed and refined using the riding model. Multi-scan method was employed for absorption correction.

Table S1: Crystallographic parameters of *Co-bpy*.

Parameters	Co (*bpy*) $(HCOO)_2$
Formula	$C_{12}\,H_{10}\,Co\,N_2\,O_4$
Formula weight (g)	305.15
Temperature (K)	273.15
Wavelength (Å)	0.71073
Crystal system	Tetragonal
Space group	*P* 4_1 2_1 2
a (Å)	7.9826(3)
b (Å)	7.9826(3)
c (Å)	17.5851(9)
α (°)	90.00
β (°)	90.00
γ (°)	90.00
V (Å^3)	1120.56(8)
Z	4
θ(deg) range for data collecn	2.80-26.41
dcalc (gcm^{-3})	1.809
μMoKα (cm^{-1})	1.543
R1 (I>2σI)	0.0147
wR2 (all)	0.0381
CCDC No.	2203219

Section S2: Crystallographic Figures and Characterization of Co-*bpy*

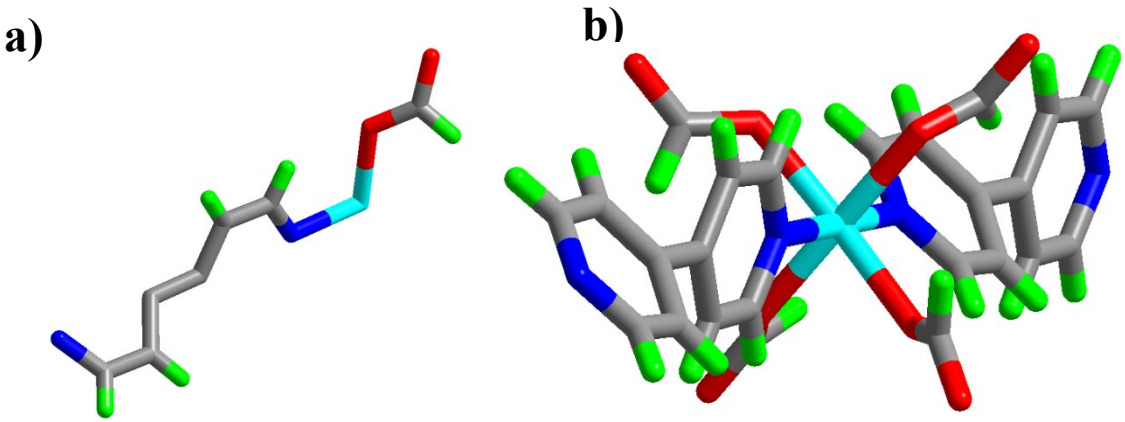

Figure S1. a) Asymmetric unit of **Co-*bpy*** and b) Coordination environment around Co(II) center, (Color code: Cobalt, sky blue; carbon, grey; nitrogen, royal blue; oxygen, red; hydrogen, green).

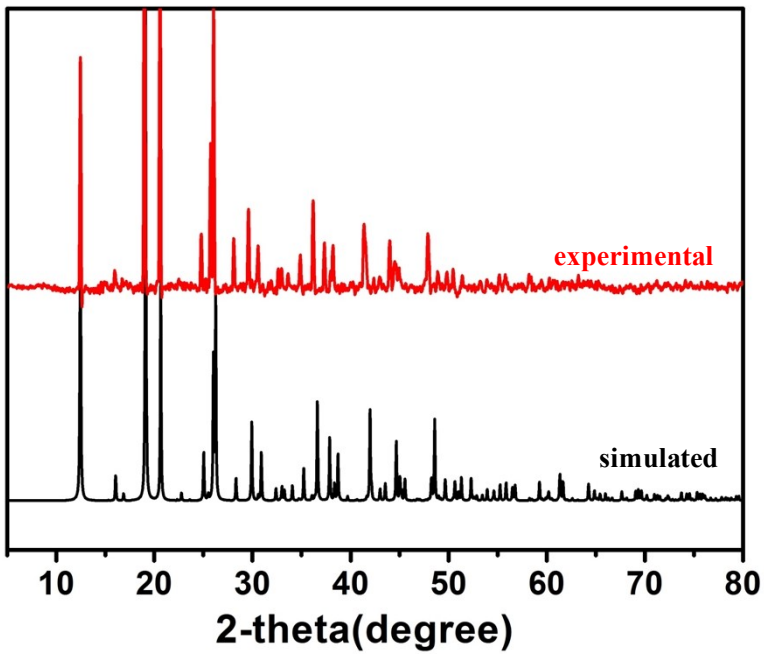

Figure S2. PXRD profiles of **Co-*bpy*** (simulated and experimental patterns)

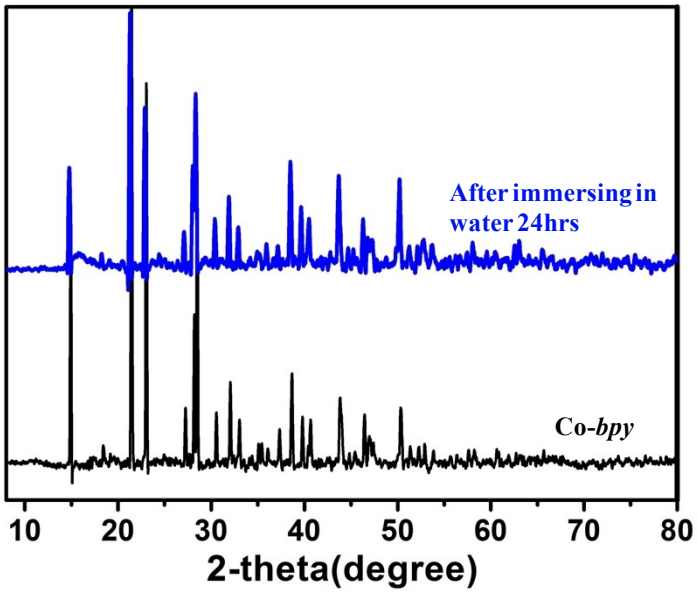

Figure S3. PXRD profiles of **Co-*bpy*** before and after immersing in water for 24hrs.

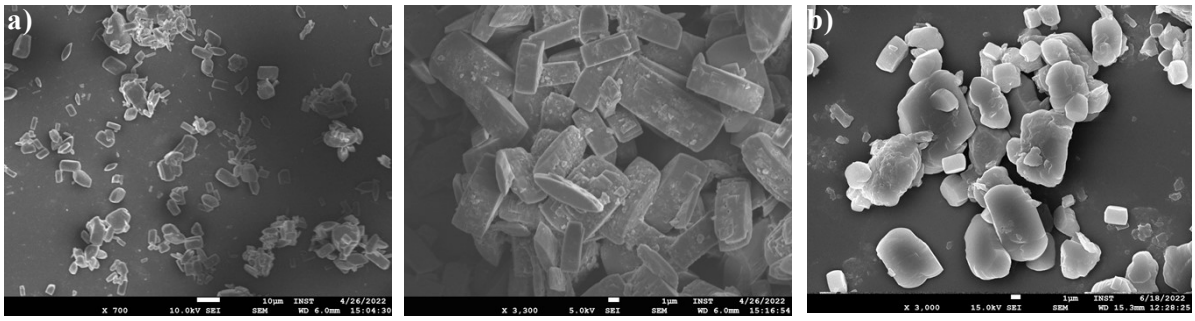

Figure S4. FESEM images of **Co-*bpy*** dispersed in a) DMF and b) H_2O.

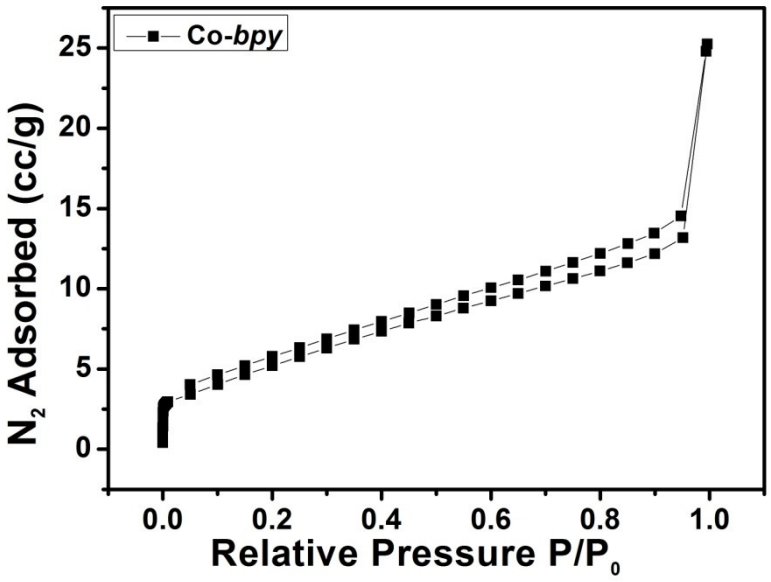

Figure S5: N_2 adsorption Isotherm of **Co-*bpy*** at 77K.

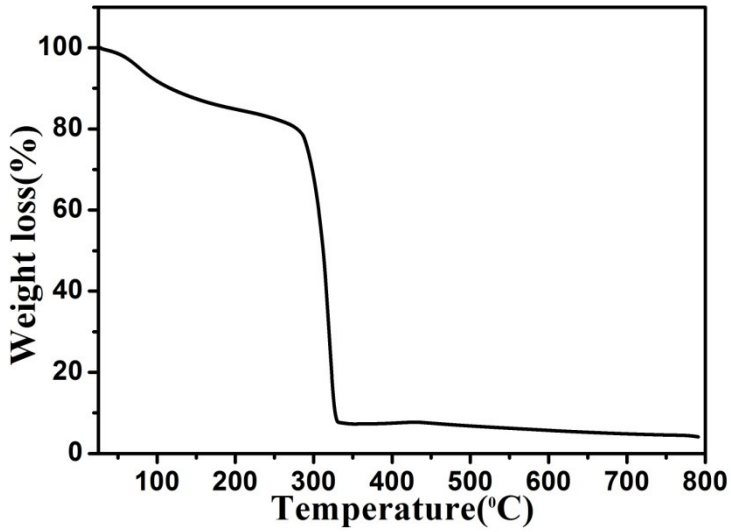

Figure S6: TGA spectra **Co-*bpy***.

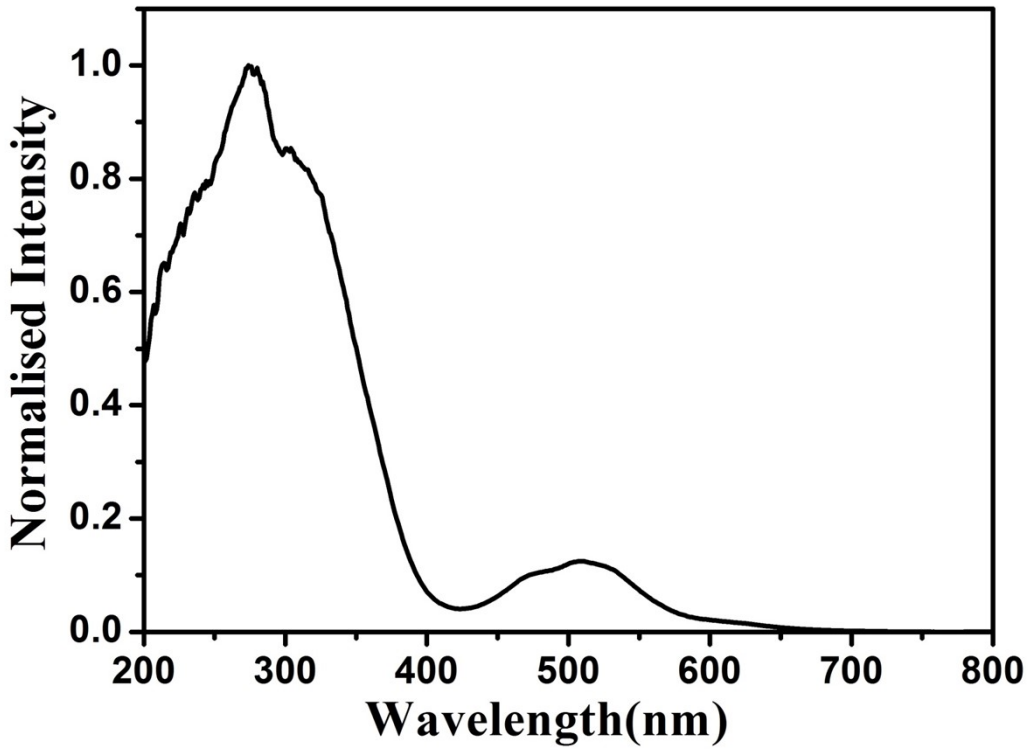

Figure S7. Solid-state UV-Vis spectrum of **Co-*bpy***.

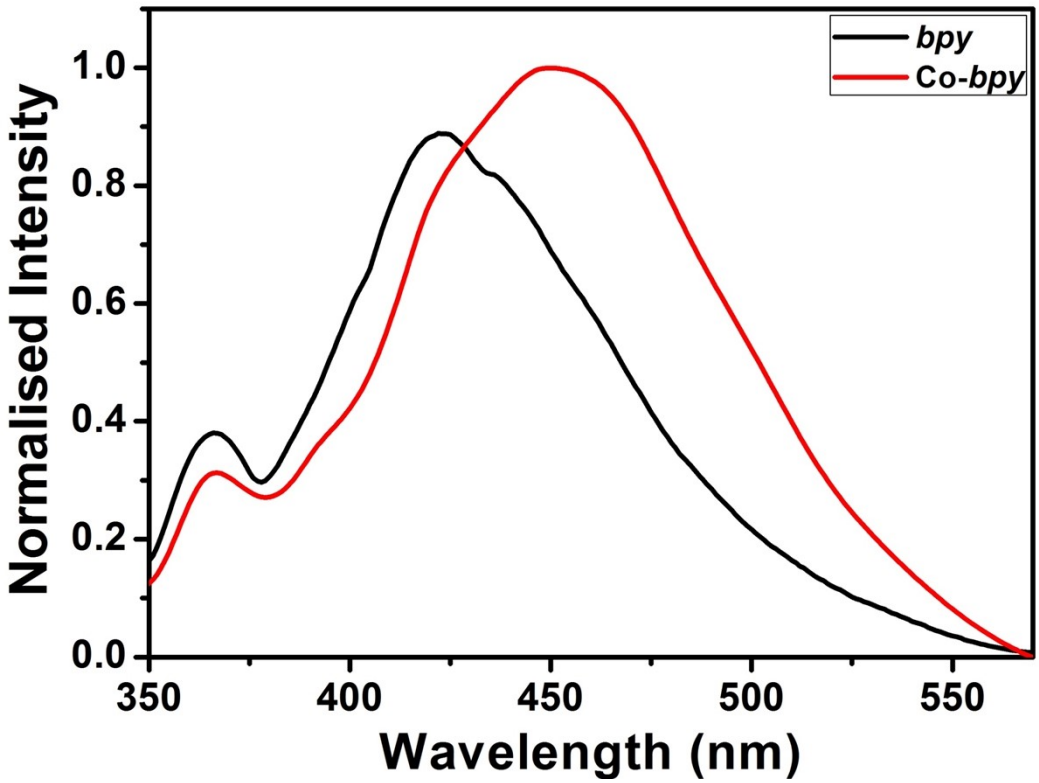

Figure S8. Emission spectra of **Co-*bpy*** and ***bpy*** ligand.

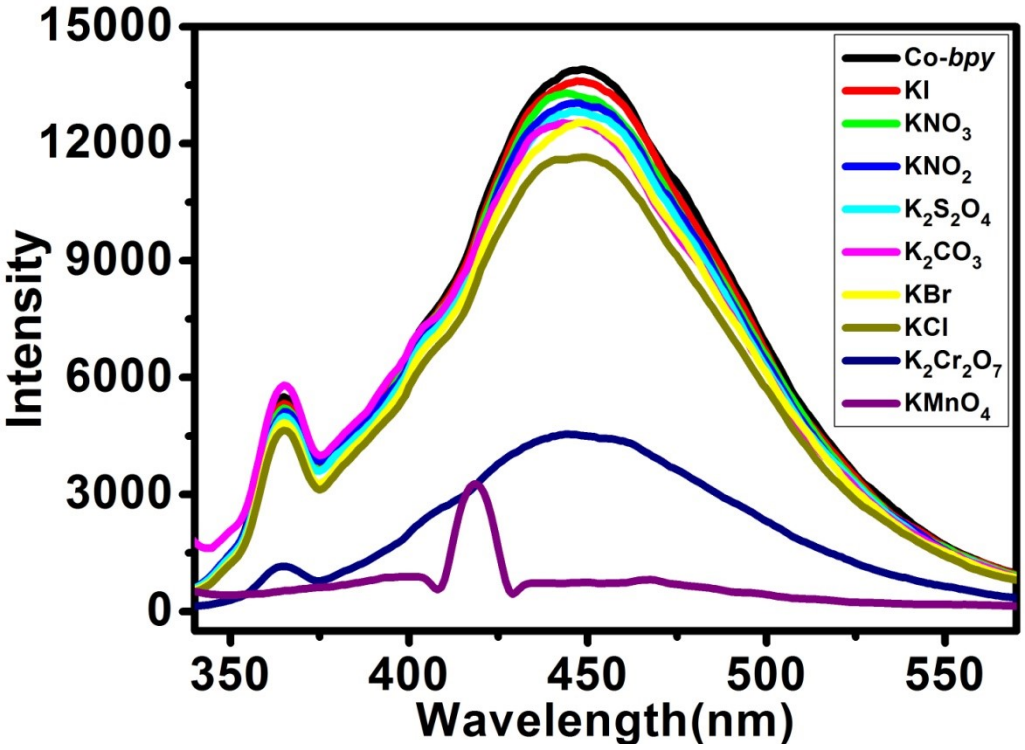

Figure S9. Emission spectra of **Co-*bpy*** in presence of different anions (0.25 mM).

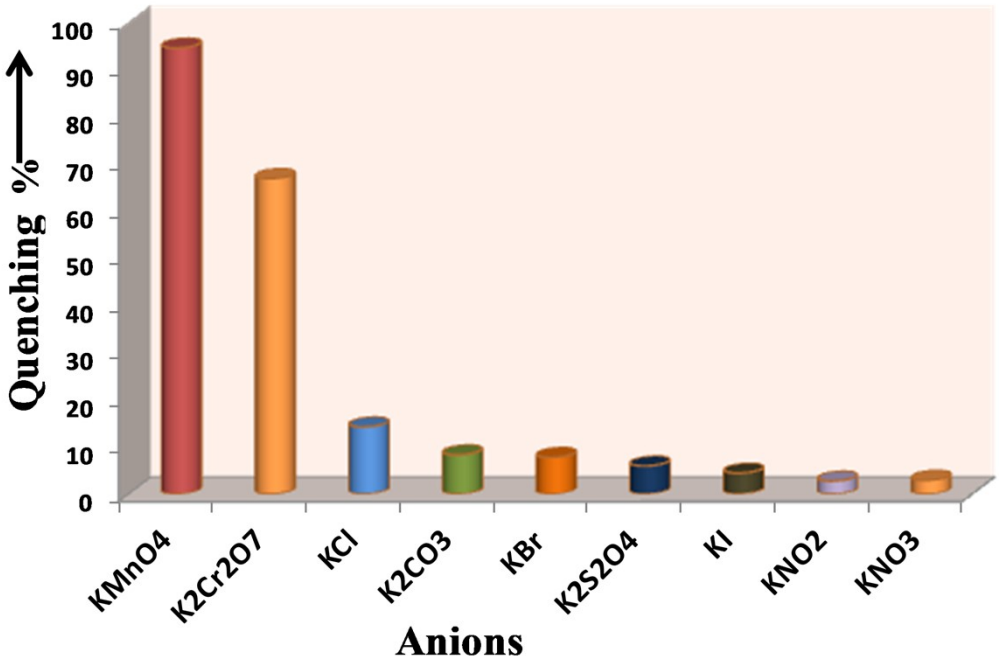

Figure S10. Bar diagram of emission intensity of **Co-*bpy*** in presence of different anions (0.25 mM).

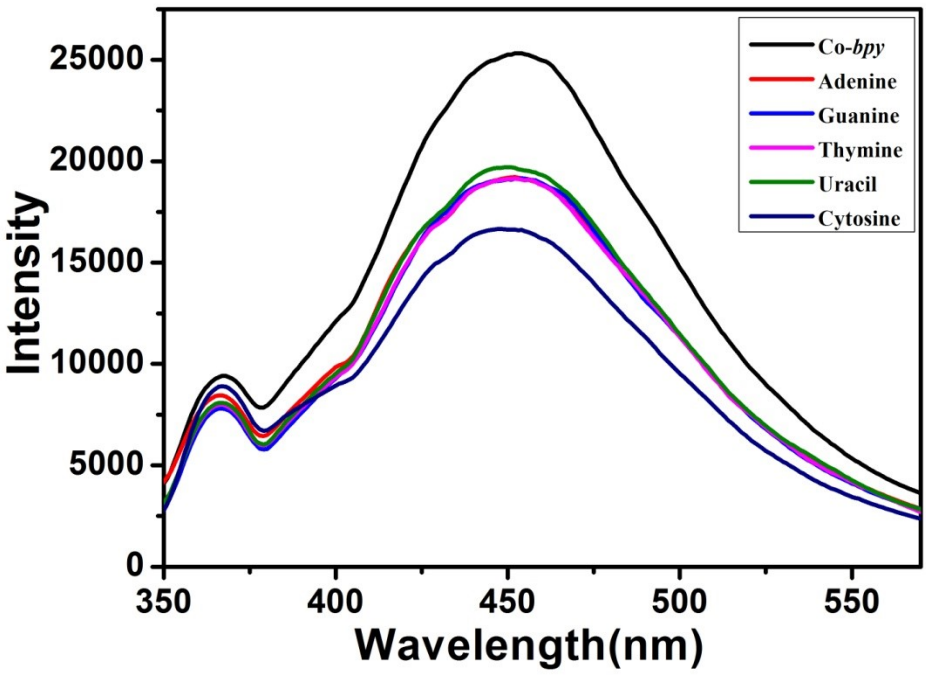

Figure S11. Emission spectra of **Co-*bpy*** in presence of Cytosine, Guanine, Thymine, Adenine and Uracil (10μM).

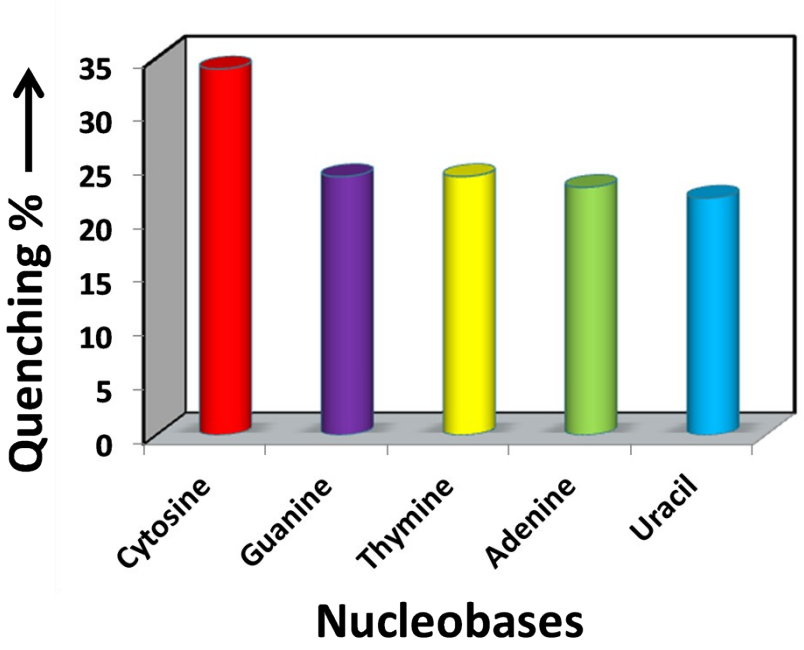

Figure S12. Bar diagram of emission intensity of **Co-*bpy*** in presence of Cytosine, Guanine, Thymine, Adenine and Uracil (10μM).

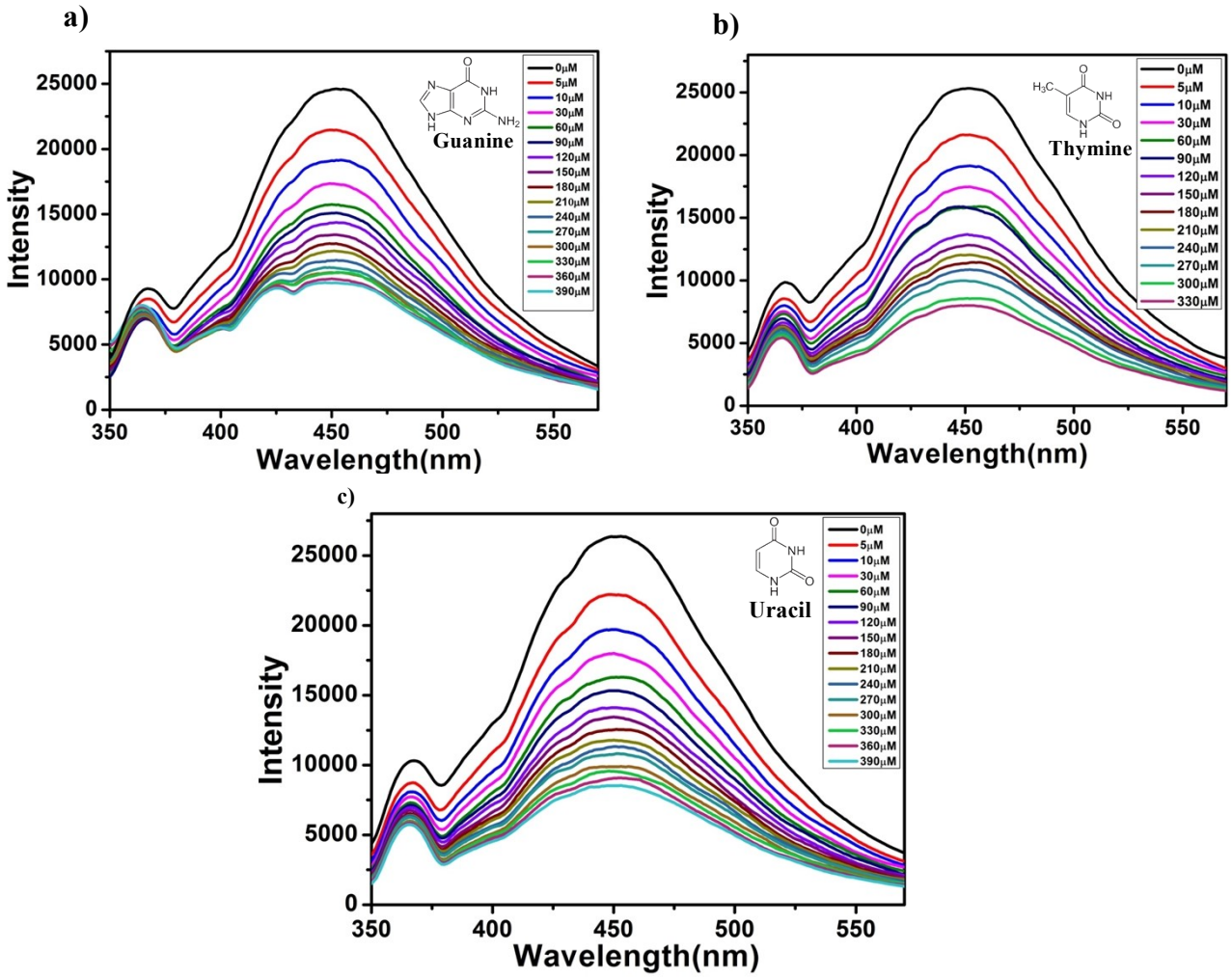

Figure S13. Change in emission spectrum of **Co-*bpy*** dispersed in water upon addition of a) Guanine b) Thymine and c) Uracil.

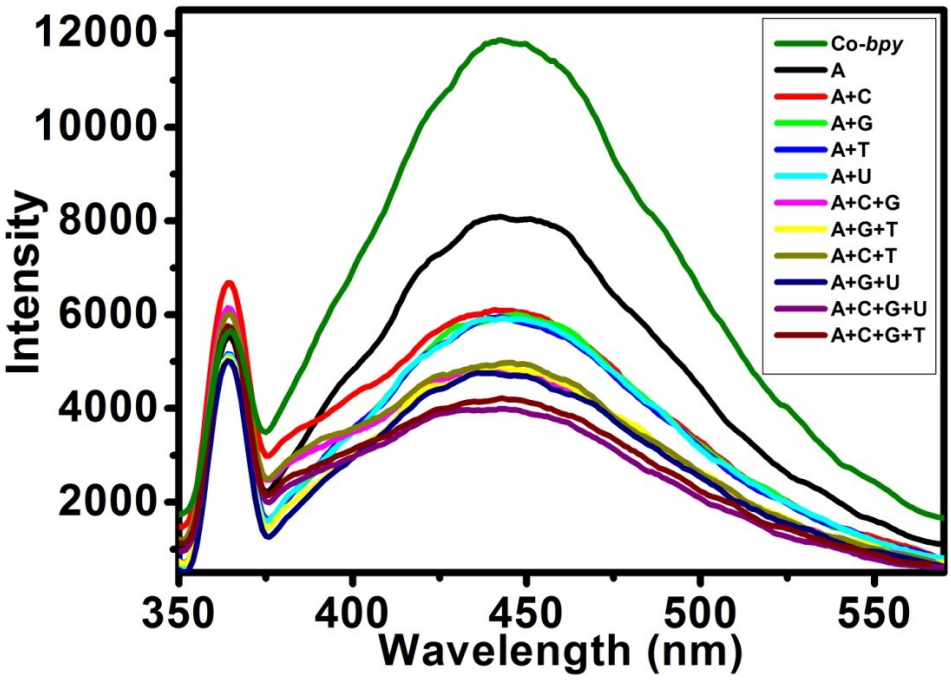

Figure S14. Change in emission spectrum of **Co-*bpy*** dispersed in water upon addition of Adenine (only) and Adenine along with other nucleobases (A- Adenine, C-Cytosine, G-Guanine, T-Thymine, U-Uracil) 10μM each.

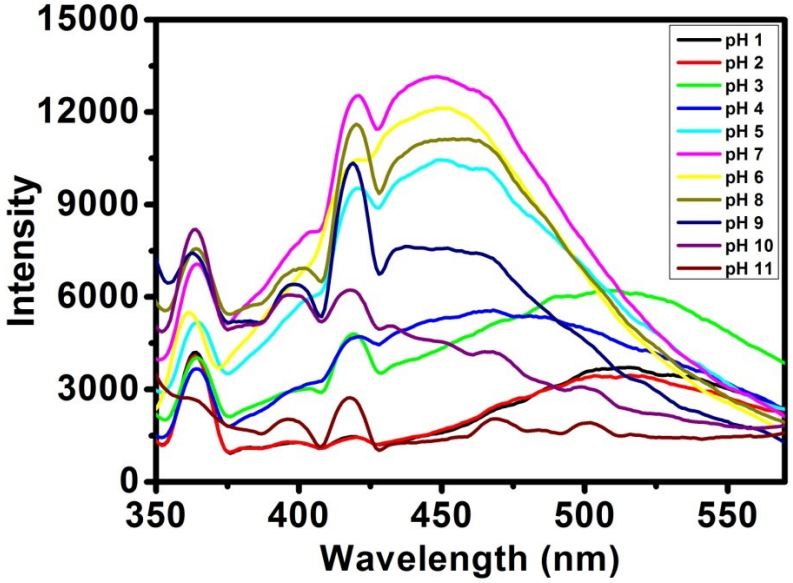

Figure S15. The fluorescence of **Co-*bpy*** at pH=1-11 solutions.

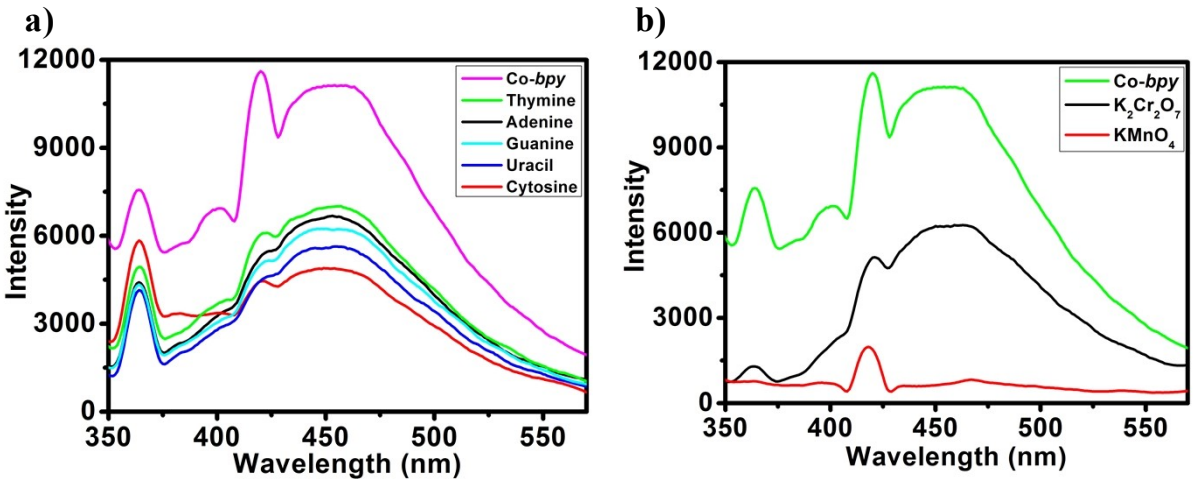

Figure S16. Change in emission spectrum of **Co-*bpy*** at pH=8 upon addition of (a) nucleobases (10µM) and (b) oxo-anions (0.25 mM).

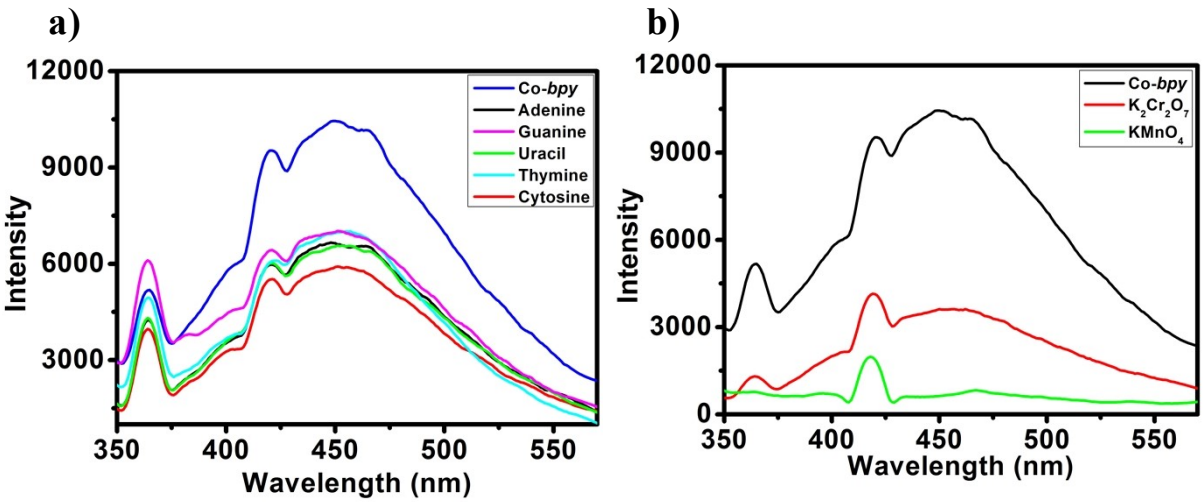

Figure S17. Change in emission spectrum of **Co-*bpy*** at pH=5 upon addition of (a) nucleobases (10µM) and (b) oxo-anions (0.25 mM).

Section S3: Detection limit calculation, determination of Stern-Volmer constant and binding constant

Detection limit was calculated using the following equation:

Detection limit = 3σ/m

Where 'σ' is the calculated standard deviation from five blank measurements and 'm' is the slope obtained from the plot of fluorescence emission with increasing concentration of analytes.

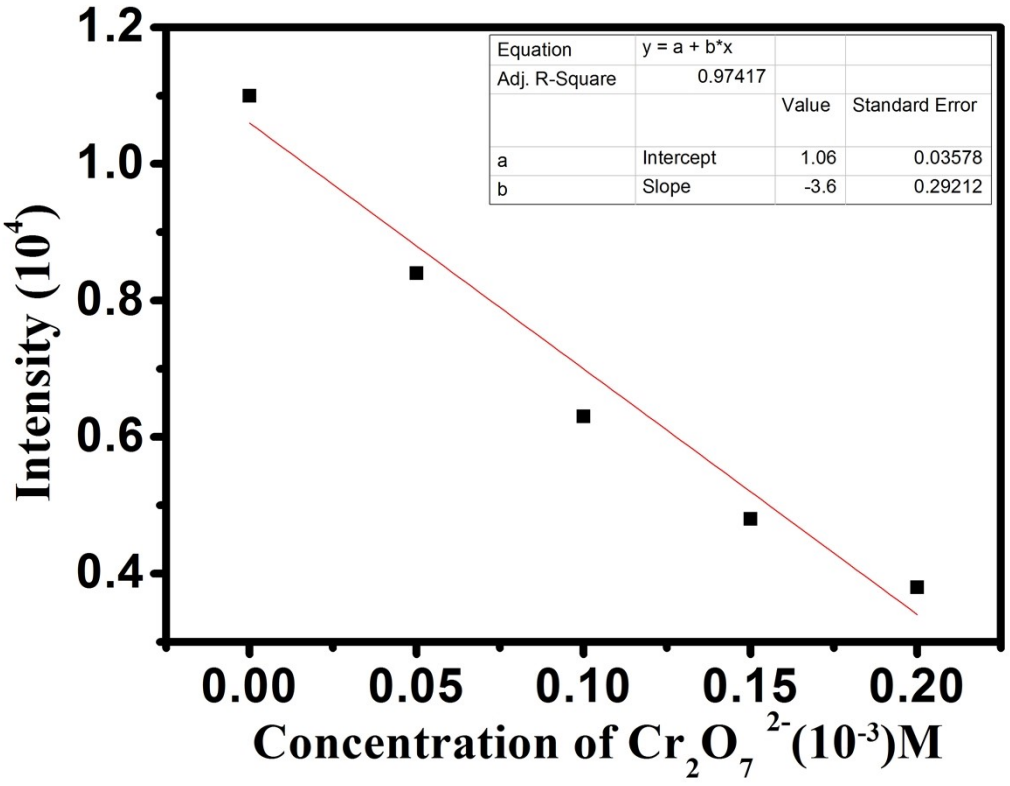

Figure S18. Determination of detection limit through fitting of the linear region of fluorescence intensity of **Co-*bpy*** upon adding different concentration of $Cr_2O_7^{2-}$ to it at λemi = 450 nm (upon λexc = 325 nm).

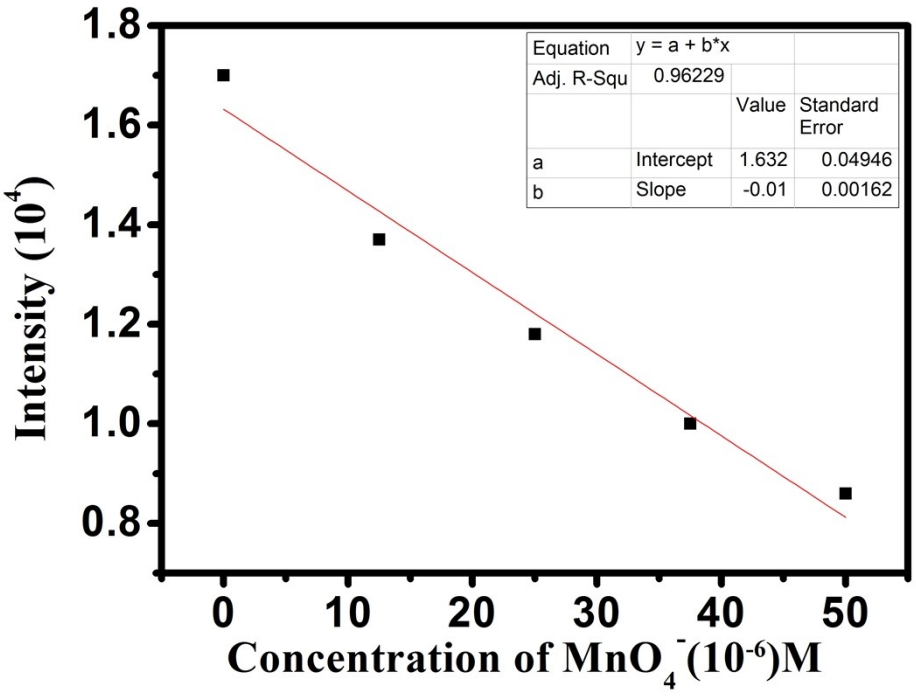

Figure S19. Determination of detection limit through fitting of the linear region of fluorescence intensity of **Co-*bpy*** upon adding different concentration of MnO_4^- to it at λemi = 450 nm (upon λexc = 325 nm).

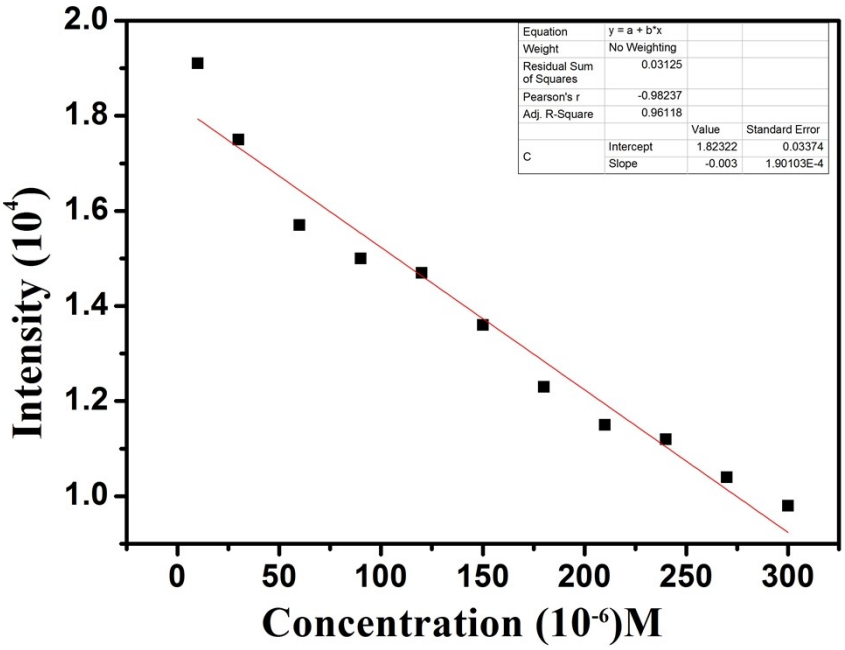

Figure S20. Determination of detection limit through fitting of the linear region of fluorescence intensity of **Co-*bpy*** upon adding different concentration of Adenine to it at λ_{emi} = 450 nm (upon λ_{exc} = 325 nm).

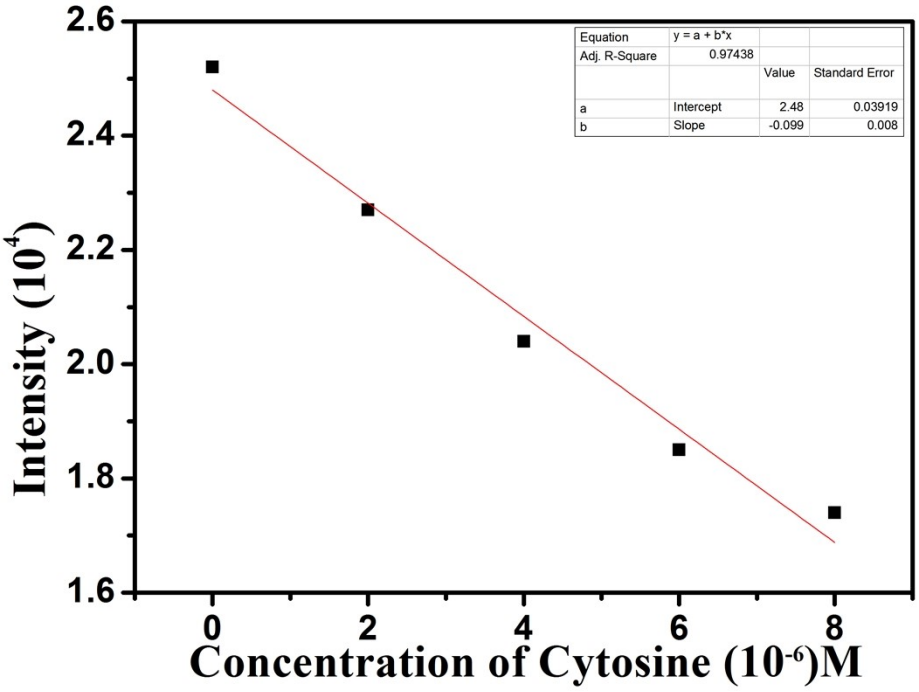

Figure S21. Determination of detection limit through fitting of the linear region of fluorescence intensity of **Co-*bpy*** upon adding different concentration of Cytosine to it at λ_{emi} = 450 nm (upon λ_{exc} = 325 nm).

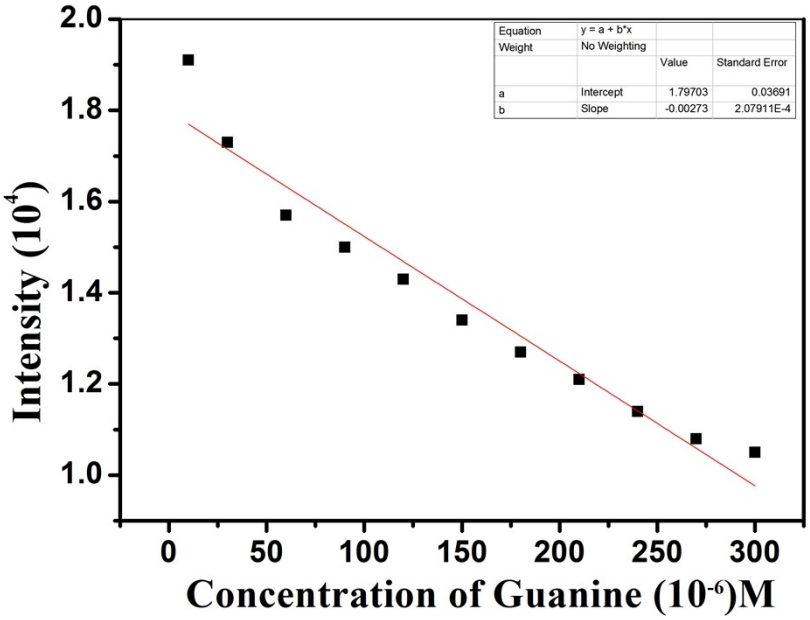

Figure S22. Determination of detection limit through fitting of the linear region of fluorescence intensity of **Co-*bpy*** upon adding different concentration of Guanine to it at λ_{emi} = 450 nm (upon λ_{exc} = 325 nm).

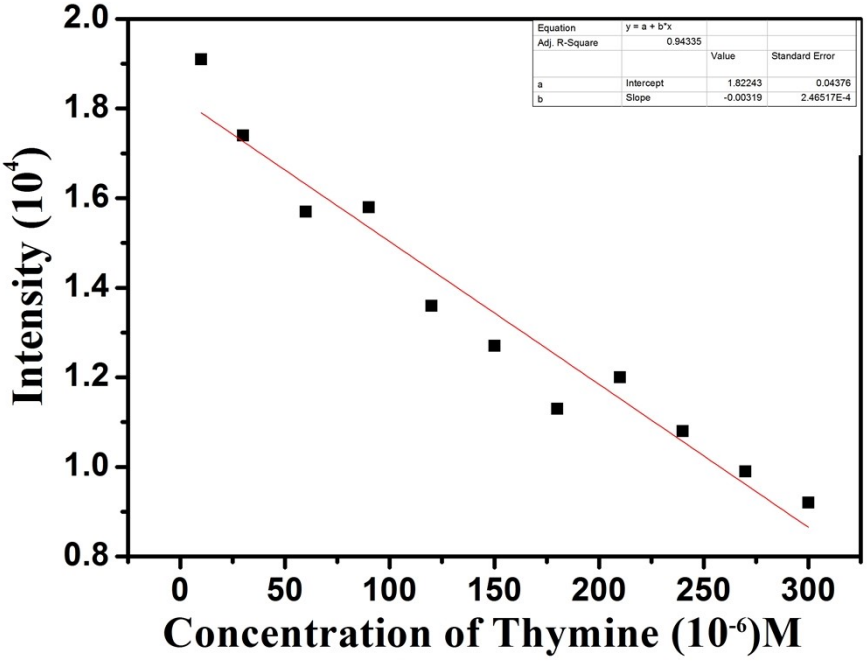

Figure S23. Determination of detection limit through fitting of the linear region of fluorescence intensity of **Co-*bpy*** upon adding different concentration of Thymine to it at λ_{emi} = 450 nm (upon λ_{exc} = 325 nm).

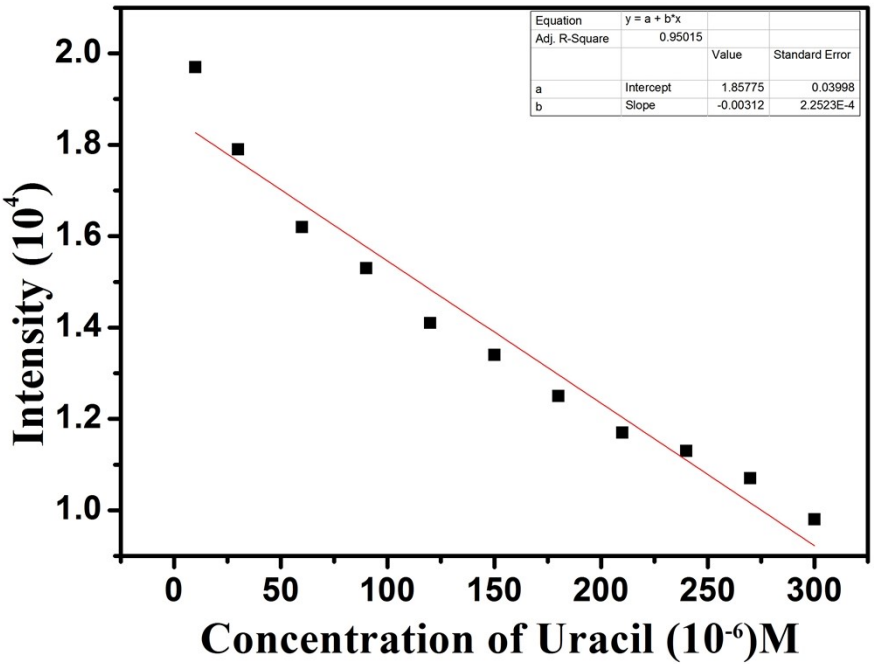

Figure S24. Determination of detection limit through fitting of the linear region of fluorescence intensity of **Co-*bpy*** upon adding different concentration of Uracil to it at λ_{emi} = 450 nm (upon λ_{exc} = 325 nm).

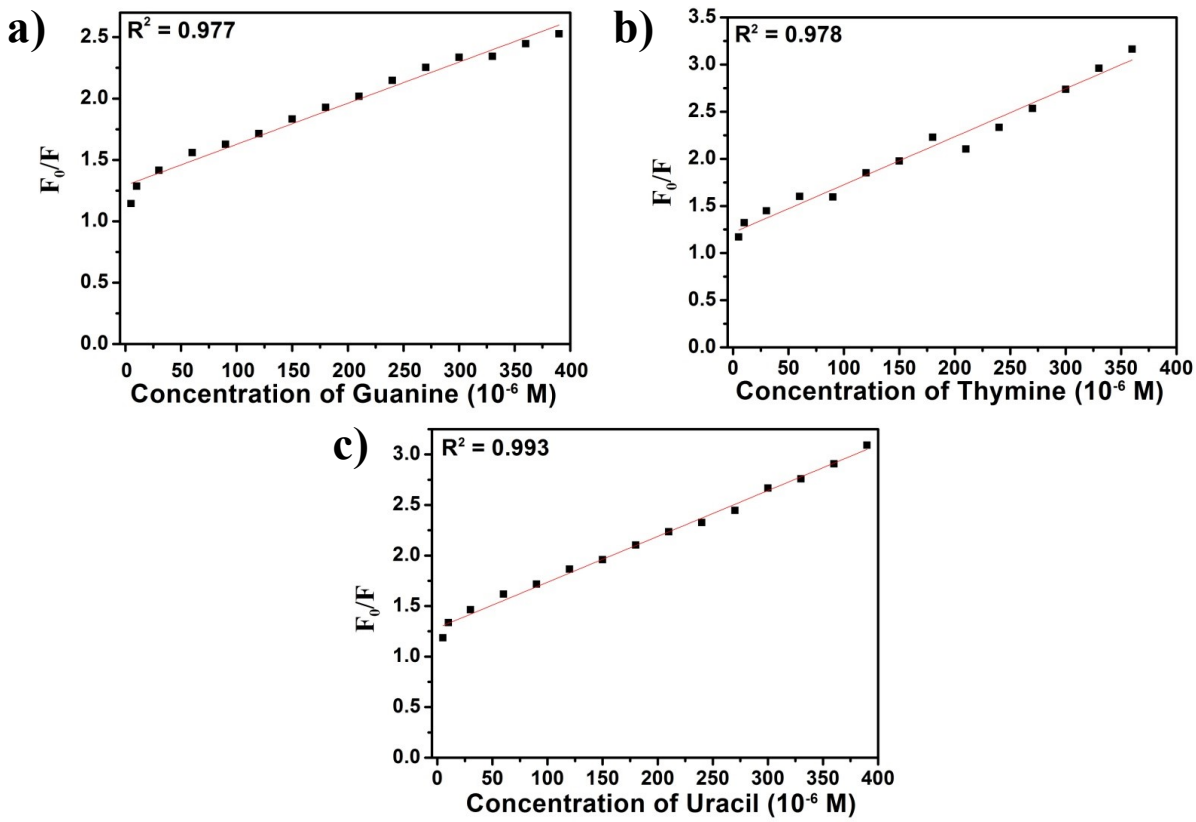

Figure S25. Stern-Volmer (SV) plot for a) Guanine, b) Thymine and c) Uracil in **Co-*bpy***.

Section S4: UV-*Vis* absorbance spectral overlap, Lifetime measurements and Recyclability plot

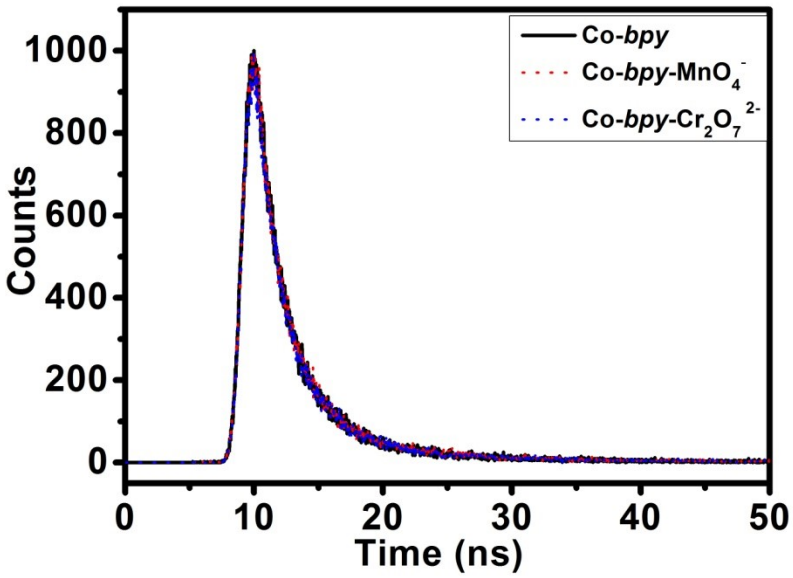

Figure S26. Lifetime decay profiles of **Co-*bpy*** before and after addition $K_2Cr_2O_7$ and $KMnO_4$.

Table S2. Average lifetimes of **Co-*bpy*** before and after addition $K_2Cr_2O_7$ and $KMnO_4$.

	Co-*bpy*(1)	**1+$K_2Cr_2O_7$**	**1+ $KMnO_4$**
τ_1 (ns)	2.09	1.76	1.70
α_1	0.75	0.54	0.68
τ_2 (ns)	8.31	7.06	6.81
α_2	0.24	0.45	0.31
$<\tau>$ (ns)	5.57	5.85	5.01

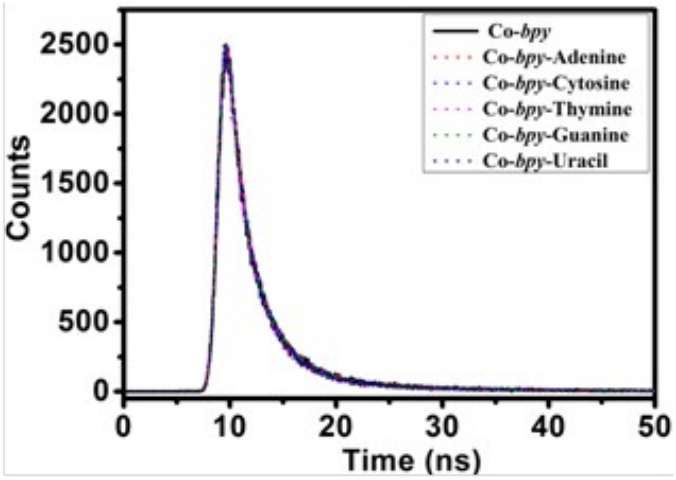

Figure S27. Lifetime decay profiles of **Co-*bpy*** before and after addition Adenine, Cytosine, Thymine, Guanine and Uracil.

Table S3. Average lifetimes of **Co-*bpy*** before and after addition Adenine, Cytosine, Thymine, Guanine and Uracil.

	Co-*bpy*(1)	**1+Adenine**	**1+ Cytosine**	**1+ Thymine**	**1 + Guanine**	**1+ Uracil**
τ_1 (ns)	2.09	2.09	2.09	2.09	2.10	2.05
α_1	0.75	0.75	0.77	0.77	0.77	0.75
τ_2 (ns)	8.31	8.16	8.18	7.99	8.00	7.67
α_2	0.24	0.24	0.23	0.23	0.23	0.25
$<\tau>$ (ns)	5.57	5.46	5.38	5.27	5.28	5.15

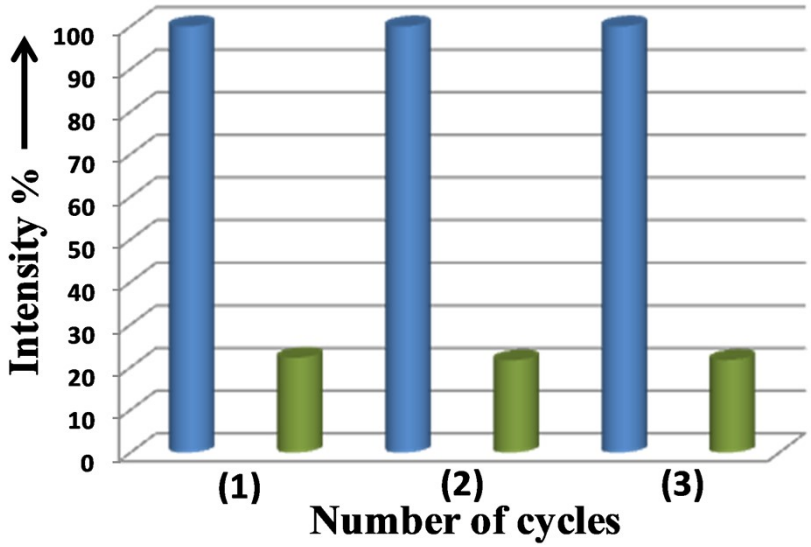

Figure S28. Recyclability plot of **Co-*bpy*** for three consecutive cycles in presence of $K_2Cr_2O_7$ (blue bar represents emission intensity before addition of $K_2Cr_2O_7$ and green bar represents emission intensity after addition of $K_2Cr_2O_7$ (0.5mM).

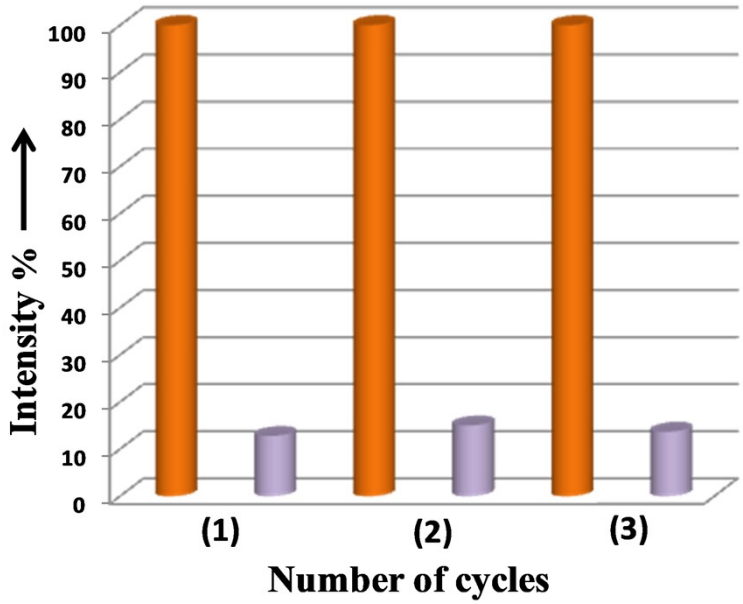

Figure S29. Recyclability plot of **Co-*bpy*** for three consecutive cycles in presence of $KMnO_4$ (orange bar represents emission intensity before addition of $KMnO_4$ and purple bar represents emission intensity after addition of $KMnO_4$ (0.125 mM).

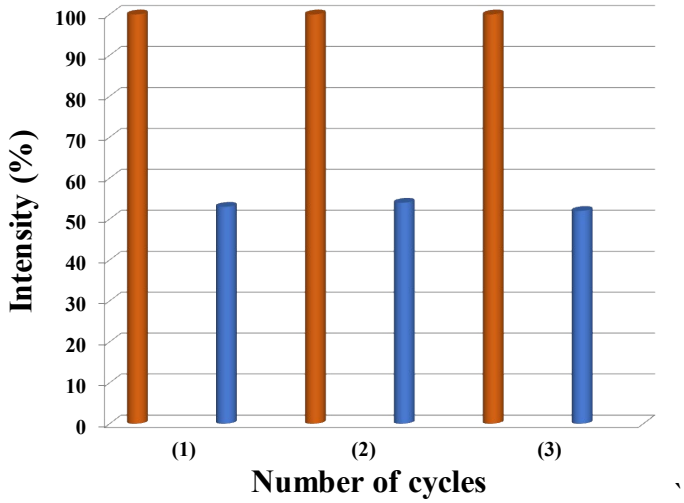

Figure S30. Recyclability plot of **Co-*bpy*** for three consecutive cycles in presence of Cytosine (brown bar represents emission intensity before addition of Cytosine and blue bar represents emission intensity after addition of Cytosine (500µL, 26µM)).

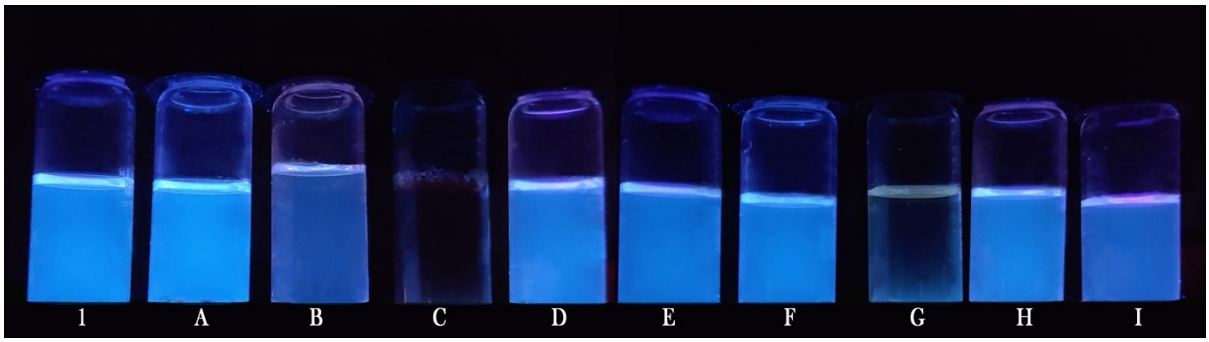

Figure S31. Sample vial images of **Co-*bpy*** in the absence and presence of 50 µL (1 mM) concentration of different analytes [where (1) Co-*bpy*; (A) KI; (B) KCl; (C) $KMnO_4$; (D) K_2CO_3; (E) KNO_2; (F) KNO_3; (G) $K_2Cr_2O_7$; (H) $K_2S_2O_4$ and (I) KBr] after UV light illumination (λ = 365 nm).

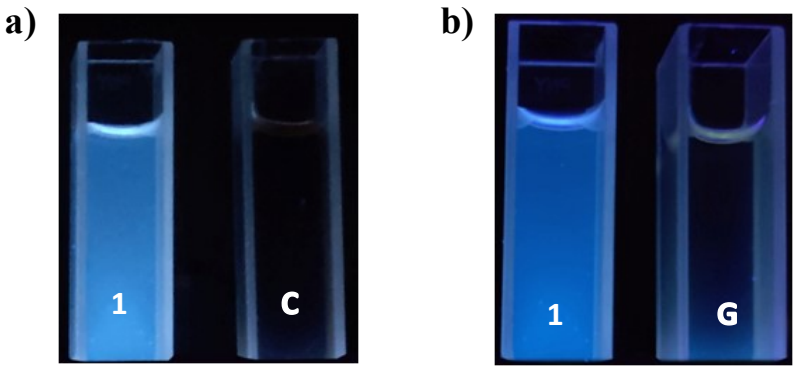

Figure S32. Cuvette vial images of **Co-*bpy*** in the absence 1 and presence of 50 µL (1 mM) concentration of C- $KMnO_4$ and G- $K_2Cr_2O_7$ under UV light illumination (λ = 365 nm).

Table S4. Comparison of "Turn-Off" fluorescent property of **Co-*bpy*** MOF for sensing Oxo-anions with literature data

Probe	Detection Limit (M)	Medium	Ref.
MnO_4^-			
$[Zn(modbc)_2]_n$	0.15×10^{-6}	DMF+H_2O	4
$\{[Zn_6Cl_6(2,2'dbpt)_3]\cdot 6H_2O\}_n$	6.14×10^{-6}	(DMF: H_2O)(1:1)	5
$\{[Cd(ttpe)(H_2O)(ip)].\ 4H_2O.DMAC\}_n$	0.34×10^{-6}	H_2O	6

$[Ni_2(\mu 2OH)(azdc)(tpim)](NO_3)\cdot 6DMA\cdot 6MeOH$	0.26×10^{-6}	H_2O	7
$[CdQ_2(H_2O)_2]$	141×10^{-9}	H_2O	8
$\{Tb(L8)_{1.5}(H_2O)_{4.5}]_n\ H_2O$	3.90×10^{-7}	H_2O	9
$[Cd(L9)(L10)].H_2O$	2.56×10^{-4}	H_2O	10
JXUST-9	1.23×10^{-6}	H_2O	11
Co-*bpy* MOF	9.5×10^{-7}	H_2O	Present Work
$Cr_2O_7^{2-}$			
$[Zn(modbc)_2]_n$	0.43×10^{-6}	DMF+H_2O	4
$\{[Zn_6Cl_6(2,2'dbpt)_3]\cdot 6H_2O\}_n$	13.64×10^{-6}	(DMF: H_2O)(1:1)	5
$\{[Cd(ttpe)(H_2O)(ip)].4H_2O.DMAC\}_n$	0.09×10^{-6}	H_2O	6
$[Ni_2(\mu 2OH)(azdc)(tpim)](NO_3)\cdot 6DMA\cdot 6MeOH$	0.95×10^{-6}	H_2O	7
$[CdQ_2(H_2O)_2]$	178×10^{-9}	H_2O	8
$\{Eu(L3)(H_2O)(DMA)\}_n$	6.05×10^{-5}	H_2O	12
$[Cd(L9)(L10)]\cdot H_2O$	2.78×10^{-4}	H_2O	10
JXUST-9	1.23×10^{-6}	H_2O	11
Co-*bpy* MOF	2.6×10^{-6}	H_2O	Present Work

Table S5. Comparison of "Turn-Off" fluorescent property of **Co-*bpy*** MOF for sensing Nucleobases with literature data

Probe	Detection Limit (M)	Medium	Ref.
Adenine			
Zn(II)-LCPs	4.83×10^{-6}	H_2O	13
L–Tryptophan-Cu^{2+}	0.046×10^{-6}	H_2O	14
GO–PANI	1.3×10^{-5}	H_2O	15
N–GN	8.0×10^{-5}	DMA	16
2,3-diphenyl quinoxaline nanoparticles	0.7×10^{-6}	H_2O	17
CoTPP	4.2×10^{-6}	H_2O	18
PDVTD-1	10×10^{-6}	DMF	19
Co-*bpy* MOF	3.1×10^{-6}	H_2O	Present Work
Guanine			
CDs	0.67×10^{-7}	H_2O	20

CdTe nanoparticles	8×10^{-8}	H_2O	21
Cu^{2+}-nuclear	1.9×10^{-6}	H_2O	22
Zn(II)-LCPs	5.97×10^{-6}	H_2O	13
Co-*bpy* MOF	3.5×10^{-6}	H_2O	Present Work
Thymine			
bis-BODIPY derivatives	1.53×10^{-6}	DMSO/H_2O	23
PDVTD-1	10×10^{-6}	H_2O	19
Co-*bpy* MOF	3.0×10^{-6}	H_2O	Present Work
Cytosine			
PDVTD-1	0.5×10^{-6}	H_2O	19
Co-*bpy* MOF	0.0969×10^{-6}	H_2O	Present Work
Uracil			
PDVTD-1	10×10^{-6}	H_2O	19
Co-*bpy* MOF	3×10^{-6}	H_2O	Present Work

References:

1. Bruker Analytical X-ray Systems, SMART: Bruker Molecular Analysis Research Tool, Version 5.618; Bruker AXS: Madison, WI2000.
2. G. M. Sheldrick, "SAINT-NT, version 6.04." Bruker Analytical X-ray Systems: Madison, WI2001.
3. Bruker Analytical X-ray Systems, SHELXTL-NT, Version 6.10; Bruker AXS: Madison, WI2000.
4. Y. Wu, D. Liu, M. Lin and J. Qian, *RSC Adv.,* 2020, **10**, 6022-6029.
5. Y. Cao, Y. Zhang, L. W. Gu, X. M. Qin, H. Y. Li, H. D. Bian and F. P. Huang, *New J. Chem.,* 2020, **44**, 10681-10688.
6. Z. X. Wang, H. X. Tian, M. Li, M. Zha, B. L. Li and B. Wu, *Appl. Organomet. Chem.,* 2020, **34**, 5977.
7. R. Goswami, G. Nilanjan, N. Seal, S. R. Dash, A. Tyagi and S. Neogi, *ACS Appl. Mater. Interfaces*. 2019, **11**, 43, 40134–40150.
8. D. B. Kanzariya, T. S. Khan, S. Das, P. Lama, R. Bandyopadhyay and T. K. Pal, *Dalton Trans.,* 2022, **51**, 7436-7454.
9. Z. L. Ma, J. Y. Shi, M. C. Wang and L. Tian, *Dyes Pigm.,* 2021, **185**, 108930.
10. G. H. Liu, Y. Li, J. Chi, N. Xu, X. L. Wang, H. Y. Lin, B. K. Chen and J. R. Li, *Dalton Trans.,* 2020, **49**, 737-749.

11. Q. Q. He, S. L. Yao, T. F. Zheng, H. Xu, S. J. Liu, J. L. Chen, N. Li, H. R. Wen, *CrystEngComm*., 2022, **24**, 1041-1048.
12. Y. T. Yan, W. Y. Zhang, F. Zhang, F. Cao, R. F. Yang, Y. Y. Wang and L. Hou, *Dalton Trans.,* 2018, **47**, 1682-1692.
13. X. Wang, J. Ma, N. Xu, Y. Wang, J. Sun and G. Liu, *CrystEngComm.,* 2021, **23**, 4760.
14. R. Duan, C. Li, S. Liu, Z. F. Liu and Y. F. Li, *Spectrochim. Acta A Mol. Biomol. Spectrosc.,* 2016, **152**, 272-277.
15. S. N. Tayade, A. K. Tawade, P. Talele, S. S. Chavhan and K. K. K. Sharma, *Methods Appl. Fluoresc.,* 2019, **7**, 045002.
16. J. Li, J. Jiang, H. Feng, Z. Xu, ,S. Tang, P. Deng and D. Qian, *RSC adv.,* 2016, **6**, 31565-31573.
17. S. B. Suryawanshi, G. R. Deshmukh, A. J. Bodake and S. R. Patil, *J. emerg. technol. innov. res.,* 2020, **7**, 139–145.
18. S. Francis and L. Rajith, *J. Fluoresc*., 2021, **31**, 577–586.
19. P. Bhanja, R. Gomes and A. Bhaumik, *RSC Adv.,* 2015, **5**, 74916-74923.
20. S. Pang, Y. Zhang, C. Wu and S. Feng, *Sens. Actuators B: Chem.,* 2016, **222**, 857–863.
21. L. Li, Y. Lu, Y. Ding, , F. Zhang and Y. Wang, *Can. J. Chem.*, 2012, **90**, 173-179.
22. Y. Cui, J. Yu and S. Feng, *Talanta*, 2014, **130**, 536-541.
23. J. Bi, X. Ji, M. Guo, H. Guo and F. Yang, *New J. Chem.,* 2019, **43**, 5890-5896.